J. Fluid Mech. (2002), *vol.* 454, *pp.* 345–364.
DOI: 10.1017/S0022112001007157 Printed in the United Kingdom

The motion generated by a rising particle in a rotating fluid – numerical solutions. Part 2. The long container case

By E. MINKOV, M. UNGARISH† AND M. ISRAELI

Computer Science Department, Technion – Israel Institute of Technology, Haifa 32000, Israel

(Received 29 June 2000 and in revised form 10 September 2001)

Numerical finite-difference results from the full axisymmetric incompressible Navier–Stokes equations are presented for the problem of the slow axial motion of a disk particle in an incompressible, rotating fluid in a long cylindrical container. The governing parameters are the Ekman number, $E = \nu^*/(\Omega^* a^{*2})$, Rossby number, $Ro = W^*/(\Omega^* a^*)$, and the dimensionless height of the container, $2H$ (the scaling length is the radius of the particle, a^*; Ω^* is the container angular velocity, W^* is the particle axial velocity and ν^* the kinematic viscosity). The study concerns the flow field for small values of E and Ro while HE is of order unity, and hence the appearance of a free Taylor column (slug) of fluid 'trapped' at the particle is expected. The numerical results are compared with predictions of previous analytical approximate studies. First, developed (quasi-steady-state) cases are considered. Excellent agreement with the exact linear ($Ro = 0$) solution of Ungarish & Vedensky (1995) is obtained when the computational $Ro = 10^{-4}$. Next, the time-development for both an impulsive start and a start under a constant axial force is considered. A novel unexpected behaviour has been detected: the flow field first attains and maintains for a while the steady-state values of the unbounded configuration, and only afterwards adjusts to the bounded container steady state. Finally, the effects of the nonlinear momentum advection terms are investigated. It is shown that when Ro increases then the dimensionless drag (scaled by $\mu^* a^* W^*$) decreases, and the Taylor column becomes shorter, this effect being more pronounced in the rear region (μ^* is the dynamic viscosity). The present results strengthen and extend the validity of the classical drag force predictions and therefore the issue of the large discrepancy between theory and experiments (Maxworthy 1970) concerning this force becomes more acute.

1. Introduction

We consider the slow axial motion of a symmetrical particle, whose circumscribing cylinder is of radius a^* in an incompressible, rotating fluid in a cylindrical container of length $2H^*$ and radius r^*_{max} which rotates with high angular velocity Ω^* about the axis of symmetry, z, as sketched in figure 1. The particle axial velocity relative to the container is denoted by w^*_p and its (quasi) steady-state value W^* will be used as the reference velocity. Typically, the particle considered is in the middle of the container. We are interested in the velocity field, $\boldsymbol{v}^*$, and drag force, D^*. We denote by p^*, ρ^* and ν^* the reduced pressure, density and kinematic viscosity. Asterisks denote dimensional variables.

† To whom correspondence should be addressed.

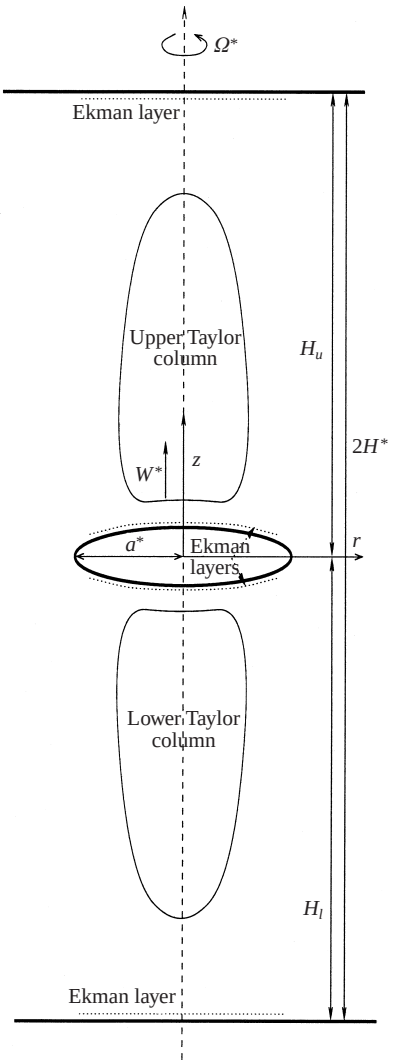

FIGURE 1. Sketch of the configuration. The particle is solid and torque-free (in the present investigation, a thin disk). The cylindrical coordinate system, whose origin is attached to the centre of the particle, co-rotates with the boundaries of the container. The lateral boundary which is at $r = r_{max}$ is not shown here. a^*, W^* and a^*/W^* are the scales for length, velocity and time t. (In addition to t, the dimensionless time $\mathscr{T}$ which is scaled with Ω^{*-1} is also used.) The z- and r-directions are called 'vertical' and 'horizontal', the corresponding velocity components are u and w, and $\psi = -\int_0^r w(r', z)r' \mathrm{d}r'$.

This is a sequel to Minkov, Ungarish & Israeli (2000), referred to as Part 1. Here we are concerned with a long container configuration where a free Taylor column (slug) may develop on the moving particle, while in Part 1 we considered the opposite short container configuration which is dominated by viscous Ekman layers and (usually thin) Stewartson layers.

From the academic aspect, this problem deserves attention because there still are significant gaps in knowledge and some unexplained discrepancies between theory and experiments. Ironically, perhaps, the present still only partly solved problem was one of the first tackled in the realm of rotating fluids at the beginning of the last century

(by Proudman, Grace and Taylor). From the practical point of view, the results are applicable to the study of rheology of rotating suspensions, centrifugal separation processes (see Ungarish 1993) and the motion of cores of planets. Nevertheless, numerical simulations of this problem are lacking.

The main dimensionless parameters of the flow field are

$$E = \frac{\nu^*}{\Omega^* a^{*2}} = \frac{1}{T}, \quad Ro = \frac{W^*}{\Omega^* a^*}, \quad H = \frac{H^*}{a^*}. \tag{1.1}$$

Here E and T are the Ekman and Taylor numbers. The Rossby number, Ro, expresses the ratio of the inertial and advective to the Coriolis accelerations in the fluid, and provides an estimate of the relative importance of the nonlinear terms in the equations of motion. We are interested in flows with small E (large T) and small Ro. In this paper we consider the case of large H so that $\delta = HE$ is of order unity. To be more specific, the numerical results are for $0.005 \leqslant E \leqslant 0.01$, $10^{-4} \leqslant Ro \leqslant 0.25$, $0.25 \leqslant HE \leqslant 0.68$.

The following scaling is utilized

$$\{\boldsymbol{r}^*, t^*, \boldsymbol{v}^*, p^*, D^*\} = \left\{a^* \boldsymbol{r}, \frac{a^*}{W^*} t, W^* \boldsymbol{v}, \frac{W^* \nu^* \rho^*}{a^*} p, W^* \nu^* \rho^* a^* D\right\}. \tag{1.2}$$

An additional scaling for the time, $\mathscr{T} = \Omega^* t^*$, is also used. The dimensionless governing equations, expressed in the system of figure 1, are

$$\nabla \cdot \boldsymbol{v} = 0, \tag{1.3}$$

$$Ro \frac{\partial \boldsymbol{v}}{\partial t} + Ro \boldsymbol{v} \cdot \nabla \boldsymbol{v} + 2\hat{\boldsymbol{z}} \times \boldsymbol{v} = -E \nabla p - E \nabla \times \nabla \times \boldsymbol{v}. \tag{1.4}$$

We assume axial symmetry. The boundary conditions are no-slip and no-penetration on the particle, whose geometry is specified, and on the container boundaries (which, in some analytical investigations, are 'at infinity'). The angular motion of the particle is defined by the torque-free condition. The vertical motion is usually assumed to be attained impulsively, but we also calculated the accelerated motion of the particle from rest under the action of a constant axial driving force, which simulates the behaviour of a buoyant particle in a gravity field parallel to the axis of rotation.

1.1. *Previous investigations*

Here we present a brief summary of previous studies on the long container configuration for the $E \ll 1$ case; the opposite, viscous flow configurations with larger values of E have been more satisfactorily covered by the existing theory and experiments (see Dennis, Ingham & Singh 1982 and the references cited therein).

The relevant analytical results are all based on the linear theory, i.e. the approximation obtained when $Ro = 0$ multiplies the advection term in (1.4). Formally, this approximation is regarded as the leading term in the expansion of the flow-field variables in powers of Ro in the asymptotic limit $Ro \to 0$ and is expected to provide good approximations to the exact solution when $Ro \ll 1$, i.e. very slow axial motion compared with $\Omega^* a^*$. We note, however, that from the physical point of view $Ro = 0$ means 'no motion' and hence the mathematical solution for this particular value of the parameter Ro cannot be realized in a laboratory experiment or in a 'numerical experiment' (like the present one) which simulates real motion. The linear theory formulation still leaves a formidable system and additional simplifications are necessary for analytical progress, such as the unbounded domain assumption. However, the time-independent, inviscid ($E = 0$) and unbounded case, considered in the second

decade of the last century by Grace, Proudman and Taylor, turned out to be an oversimplification whose solution is not unique.

Stewartson (1952) considered the inviscid, unbounded but time-dependent problem. This solution shows that the flow field reaches a steady state, where the drag force on a circular particle such as a sphere or a disk is

$$D_0^* = \tfrac{16}{3} a^{*3} \Omega^* W^* \rho^*, \tag{1.5}$$

and in dimensionless form,

$$D_0 = \tfrac{16}{3} E^{-1}. \tag{1.6}$$

Here the subscript 0 in the drag force denotes the inviscid unbounded container limit (unlike the short container case). (The presence of E^{-1} in (1.6) is due to the accepted scaling (1.2); the result is used here for comparisons at finite values of E only.) The corresponding flow field displays a cylinder of radius 1 of swirling fluid moving with the particle. This domain can be identified as the Taylor column, but the infinite length, and the fact that the swirl velocity is infinite and discontinuous on the vertical boundary, render this description unrealistic.

Morrison & Morgan (1956) and Moore & Saffman (1969, § 8), considered the steady-state slightly viscous ($E \to 0$) flow field for a disk. Only radial shear terms are kept in this approximation, i.e. the 'horizontal' Ekman layers are not incorporated and the no-slip conditions on the particle are not satisfied. The drag force calculated with this model turns out to be the same as predicted by the inviscid analysis, (1.6), but the discontinuities of the inviscid flow-field result are smoothed out by the small viscous terms. Moreover, as pointed out by Barnard & Pritchard (1975), the flow field of the Moore & Saffman approximation has a stagnation point on the axis at the distance $0.053/E$ from the particle; this was identified as the tip (and hence the length) of the Taylor column slug of fluid trapped by the particle. The shape of this column, the flow inside it and the interaction between it and the Ekman layers on the particle remained unsolved.

Experiments, notably by Taylor (1922, 1923), have demonstrated the appearance of a long column of fluid which moves with the particle, and further quantitative experimental results were given by Maxworthy (1970). The latter experiments were performed in a cylinder of about 150 cm long and 30 cm diameter with spherical particles of about 1 cm radius, and covered quite a wide range of Ro (but larger than 0.02) and E (but larger than 2×10^{-3}). The measured drag force for small values of Ro was about 50% larger than the prediction (1.6). On the other hand, the length of the Taylor column (slug), $0.058/E$, turned out to be in fair agreement with Moore & Saffman's results. This perplexing drag discrepancy and the lack of theoretical knowledge for the interpretation of the observed flow in the Taylor column (including its shape and the interaction with the Ekman layers on the particle) motivated much of the following research on this problem.

Hocking, Moore & Walton (1979) extended the Moore & Saffman model to a domain bounded axially by solid walls at $z = -H_l, H_u$ (again, the Ekman layers and the no-slip conditions were not included). The results indicate that the drag force in a bounded domain is larger than predicted by (1.6). However, the discrepancy is only about 9% when $H_u = H_l = E^{-1}$, and increases when the domain shrinks and when the asymmetry increases. No results for the flow field and Taylor column were presented.

Weisenborn (1985) used the special method of induced forces to calculate the drag on a sphere in an unbounded domain for arbitrary values of E. The viscous

contribution increases the drag but for $E \to 0$ the inviscid result (1.6) is recovered (the discrepancy is less than 9% for $E = 10^{-3}$). No information about the flow field and Taylor column was obtained.

An exact solution of the linear problem for a disk particle in an unbounded domain, for arbitrary values of E, was presented by Vedensky & Ungarish (1994, referred to herein as VU). The Ekman layer influence is implicitly incorporated in these flow field and drag force results. It turns out the Taylor column slug (both at the front and rear of the particle) is actually a closed domain of recirculation (bounded by the interfaces $\psi(r, z) = 0$) which is clearly detached from the particle and does not exchange fluid with the Ekman layers, see figure 1. The critical value of E below which such a Taylor column structure appears is $1/37$ (approximately), and for small E the length of the column is $0.051/E$. At a fixed finite E the drag force of a disk is, as expected, smaller than that of a sphere, but still larger than the inviscid result (1.6); again, the latter is recovered for very small values of E. Tanzosh & Stone (1994) presented a similar exact solution for spherical and prolate-ellipsoidal particles. For a sphere the drag force is in perfect agreement with the results of Weisenborn (1985), and the flow field is like that of the disk, but the critical E is about $1/50$. We infer that the critical E decreases with $L =$ (axial length)/radius of the particle. Conversely, we speculate that for a given E and a streamlined particle of sufficiently large L the slug-like Taylor column of trapped recirculating fluid does not appear, but such configurations are outside the scope of our investigation.

An exact solution of the linear time-independent equations of motion in the axially bounded domain for a disk particle in a symmetric position ($H_l = H_u = H$) was obtained by Ungarish & Vedensky (1995, referred to herein as UV), and shows the influence of H on the shape of the Taylor column and on the drag force for small but finite values of E. The results indicate that the Taylor column slug appears when the parameter $\delta = EH > 0.08$ and that for $\delta > 0.25$ the flow-field features in this domain are very close to those in the unbounded case.

The time-dependent behaviour of the flow field and the drag force in the unbounded inviscid case for impulsive start of a disk particle were investigated by Greenspan (1968) and Smith (1987). The former study indicates that the velocity of propagation of the tip of the Taylor column is $0.675a^*\Omega^*$, and the latter shows that the drag force develops in less than one revolution of the system. There is no confirmation of these results.

No numerical results for the problem under investigation have been presented, to our knowledge. A closely related study, Dennis *et al.* (1982), concerned a spherical particle in an unbounded domain. The steady-state axisymmetric Navier–Stokes equations in the stream-function–vorticity formulation in spherical coordinates were solved, with the far-field boundary condition applied at some finite radius. However, due to convergence difficulties, reliable results were obtained only for $E \geqslant 2$. We are interested in the opposite range, $E \ll 1$.

1.2. *Objectives*

The above-mentioned analytical and experimental studies have obvious limitations and leave open important questions, in particular concerning the time-dependent motion and the effect of the nonlinear terms on the drag and Taylor column behaviour. The possibility that the linear theory ($Ro = 0$) is a singular limit of the Navier–Stokes solution and is therefore never compatible with experimental observations (which are necessarily at $Ro > 0$) has not yet been dismissed by evidence from numerical computations of the full Navier–Stokes equations.

The objective of the present study is to throw light on these topics. To this end, we attempted the numerical solutions of the full system of Navier–Stokes equations (1.3)–(1.4), in axisymmetric form, for a disk particle in a cylindrical container, by a finite-difference method. The advantage over previous investigations is the incorporation of more relevant physical effects in the analysis, which enable us to gain wider, more reliable and more accurate results and insights.

The numerical finite-difference solver is described in Part 1. Briefly, the spatial discretization grid is non-uniform, for improving the resolution around $r = 1$ and in the Ekman layers. The horizontal grid lines are adjusted (moved) repeatedly with time to fit the relative motion of the disk with respect to the walls. The results are obtained by time marching from an initial state of solid-body rotation. The typical grid has about 150 radial and 100–400 axial intervals. Unless stated otherwise, the computations are for $r_{max} = 5$ (we found that larger values of this parameter have insignificant influence on the (quasi) steady-state features, and the influence on the transient flow will be mentioned). We noticed that the required computational resources increase drastically when EH is of the order of unity and E decreases, and therefore we had to restrict the computations to $E \geqslant 1/200$ and $H \leqslant 80$.

The paper is organized as follows. The numerical results for almost linear flows are presented and discussed in § 2 for both the steady-state and the time-dependent stage. Then, the influence of the nonlinear advection terms is considered in § 3. We present some concluding remarks in § 4.

2. Almost linear flow: numerical results with $Ro = 10^{-4}$

2.1. *The steady state*

2.1.1. *The symmetric configuration*

The first task is to perform critical comparisons of the numerical results with previous solutions obtained by different methods. The most relevant analytical results for comparisons are provided by the exact linear solution of UV for the steady-state flow in a symmetric configuration (i.e. the disk is midway between the upper and lower boundaries); for the related unbounded case the results of VU can be used.

A comparison of the drag force results between the present computations and those of UV is presented in table 1 for various values of E and H (not tabulated in the cited paper, but computed here with the same software). The values of the parameter $\delta = EH$ in this table are definitely in the range where 'long' container features are dominant, including the presence of a well-developed Taylor column. The present results are obtained by time marching until time fluctuations were judged as insignificant (see § 2.1.3), while the analytical ones use $Ro = 0$ in the time-independent momentum equations and apply boundary conditions at $r_{max} = \infty$. Nevertheless, the difference between the numerical and analytical drag force results is below 1% for all cases considered, in the range of the numerical error of the compared variables. We therefore conclude that table 1 indicates excellent agreement between the results and can be considered as a reliable mutual validation both of the exact linear solution and of the present numerical solution for the long container case.

The numerically computed meridional flow fields, in terms of the stream function $\psi(r, z)$, are displayed in figures 2(b) and 3(b), for two cases with different H and E but the same $\delta = 0.25$. The presence of a trapped region of recirculating fluid (inside the closed streamline $\psi = 0$), which we identify as the Taylor column slug, is evident. For comparison, the analytical-linear streamlines for the unbounded configuration with

E	H	$\delta = EH$	D_{a-l}	D_{num}	$\Delta(\%)$	$D_{num}/D_0 - 1$
1/100	25	0.25	776	772	−0.5	0.46
	50	0.50	696	693	−0.4	0.31
1/117	80	0.68	776	773	−0.4	0.24
1/200	50	0.25	1486	1475	−0.7	0.39

TABLE 1. The drag force results of the exact analytical-linear and present numerical computation for various E and H; Δ is the discrepancy between these results. The deviation of the numerical drag result from the unbounded inviscid prediction is given in the last column.

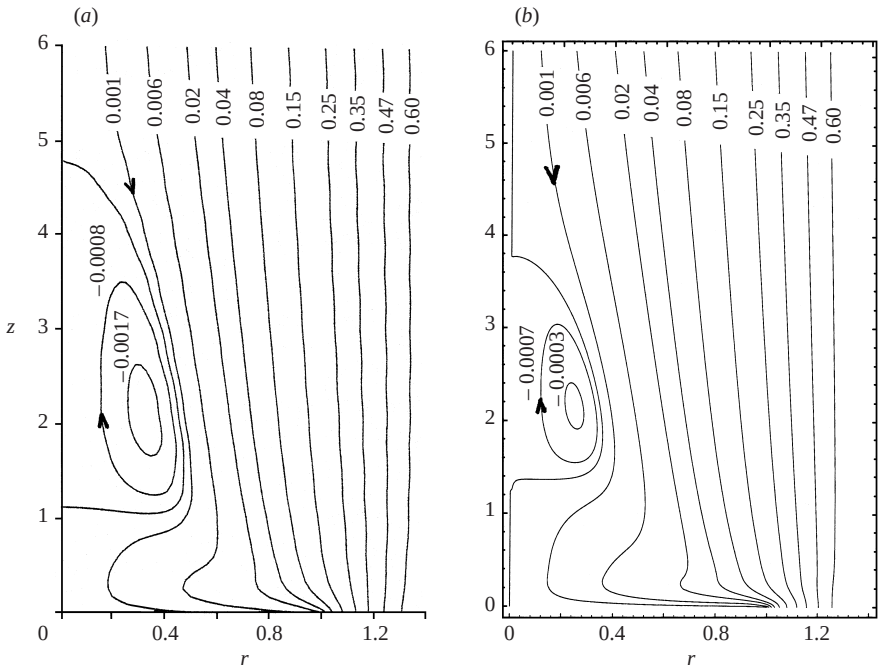

FIGURE 2. Stream function contour lines for (*a*) $E = 1/100$, $H = \infty$ (analytical linear) and (*b*) $E = 1/100$, $H = 25$, $Ro = 10^{-4}$ (numerical). The computation was performed on a 193×147 grid with 300 000 time steps.

the same value of E are displayed in figures 2(*a*) and 3(*a*). The qualitative features of the numerical results are in full agreement with the prediction of the analytical-linear solution. UV found that for small E and $\delta \geqslant 0.25$ the flow fields in bounded and unbounded containers are very similar. Here we observe that at $\delta = 0.25$ some influence from the boundaries is still present: the length of the Taylor column is shorter than in the infinite case (3.8 instead of 4.8 for $E = 1/100$ and 8.1 instead of 9.8 for $E = 1/200$) and the recirculation is weaker. We attribute this to the fact that E is not truly small; indeed, as E decreases, the relative discrepancy decreases.

2.1.2. *The asymmetric configuration*

For the configuration with the disk in a non-symmetric position, $H_l \neq H_u$, no analytical linear results are available for a direct accurate comparison. The only relevant study is that of Hocking *et al.* (1979) which calculated the drag force on a disk using the linear steady-state equations from which the axial shear has been

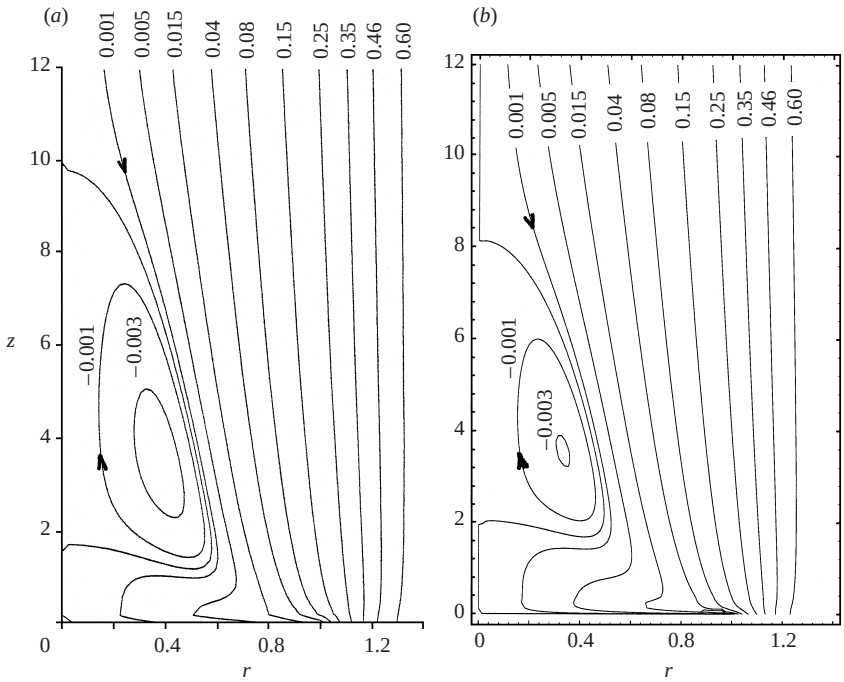

FIGURE 3. Stream function contour lines for (*a*) $E = 1/200$, $H = \infty$ (analytical linear) and (*b*) $E = 1/200$, $H = 50$, $Ro = 10^{-4}$ (numerical). The computation was performed on a 443×147 grid with 300 000 time steps.

discarded; it predicts that, in the limit $E \to 0$, the ratio of the drag in the bounded domain to the drag in the unbounded domain is a function of δ_u and δ_l only (the subscripts t and b are used in that paper instead of the present u and l); let us denote this function by $G(\delta_u, \delta_l)$. However, some modifications are necessary to make these results useful in realistic (finite E) circumstances, as follows.

Let $D(E, H_u, H_l)$ and $D(E, \infty)$ be the drag force, in the asymmetric configuration and in the unbounded domain respectively, for some value of E. Following the results of UV for the symmetric case, for small but finite E and for $\delta_u + \delta_l > 0.16$, we suggest the conjecture

$$D(E, H_u, H_l) = G(\delta_u, \delta_l) D(E, \infty). \tag{2.1}$$

The values for $D(E, \infty)$ (denoted in brief D_∞) are available analytically by the method of VU and $G(\delta_u, \delta_l)$ are provided by Hocking *et al.* (see Appendix A).

The conjecture (2.1) is used in table 2 to estimate the analytical linear drag, which is displayed together with the present numerical drag results for typical configurations. As in the symmetric case, the numerical drag is slightly smaller than the analytical prediction, by about 1%. The asymmetry with respect to the boundaries increases the drag, but this is a small contribution compared with the drag increase produced by the presence of the boundaries. The agreement between the predicted and the computed results is good (also for cases not displayed here), which we consider to be a verification both of the numerical results and of the conjecture (2.1).

2.1.3. *The time-dependent development of the flow field for an impulsive start*

We now analyse the transient flow field for the impulsive start of the disk from rest (i.e. solid-body rotation of the fluid–disk–boundary system) until the attainment of the steady-state features.

E	H	δ_u	δ_l	$D_{\infty a-l}$	$D_{\infty a-l}G(\delta_u, \delta_l)$	D_{num}	$\Delta(\%)$
1/100	50	0.50	0.50	597	697	693	−0.6
		0.33	0.67	597	714	707	−1.0
		0.25	0.75	597	727	730	−1.6
1/117	80	0.68	0.68	690	776	773	−0.4
		0.52	0.84	690	784	779	−0.6
		0.41	0.96	690	799	791	−1.1

TABLE 2. Effect of asymmetry on drag force results, according to the analytical linear conjecture (2.1) and present numerical computations (with $Ro = 10^{-4}$). Δ is the discrepancy, $\delta_u = EH_u, \delta_l = EH_u$.

Consider first the drag force behaviour. The relevant analytical study of Smith (1987), for a disk in an unbounded domain and $E = 0$, yields the elegant result

$$\frac{D_0(\mathscr{T})}{D_0(\infty)} = \int_0^{2\mathscr{T}} J_0(u)\,\mathrm{d}u, \tag{2.2}$$

where J_0 is the Bessel function of order zero, and we recall that $\mathscr{T}$ is the time scaled with Ω^{*-1}. According to this formula, the drag increases quickly and first overshoots its steady-state value by about 47% at $\mathscr{T} = 1.2$ (about 0.2 revolutions of the system); the convergence to the steady-state value is within (almost inertial, slowly damped) oscillations with period of about π.

Our numerical results, figures 4 and 5, confirm that the drag grows quickly, displays an initial overshoot at about 0.2 revolution, and then damped oscillations. However, there are quantitative discrepancies with (2.2), being most pronounced in the amplitude of the oscillations: the first overshoot is only about 5%. While viscous effects are expected to reduce this amplitude overshoot, the difference is still surprisingly large. The period of the oscillations is larger by about 30%, and this too can be attributed to the influence of viscosity, as the damping can be seen to be faster for $E = 1/100$ than for $E = 1/200$.

After the first revolution ($\mathscr{T} = 2\pi$) the drag force attains a quasi-constant average value which does not depend on H. A closer examination indicates that this is the value of the drag predicted for the infinite container by VU (597 for $E = 1/100$ and 1145 for $E = 1/200$). This quasi-constant value of the drag persists for a period of time that depends on H: about 2.5 revolutions for $H = 25$ and about 5 revolutions for $H = 50$. We infer that during this first stage the flow created by the disk 'does not know' that the container is bounded axially.

This inference is supported by the behaviour of the Taylor column as a function of time, which is considered next. The relevant previous investigation by Greenspan (1968, § 4.3) considers the time-dependent inviscid ($E = 0$) flow field created by the impulsively started disk in an unbounded domain. The solution points out that the time-dependent Taylor column is a manifestation of the basic mechanism of inertial wave propagation, with radial phase velocity and axial group velocity. In the Taylor column formation the important part of the spectrum consists of wavelengths of (approximately) the diameter of the disk. In particular, the position of the stagnation point of the flow towards the disk, which can be identified as the tip of the Taylor column, propagates with the velocity $0.675\Omega^* a^*$ and corresponds to a wavelength of 2.12. This prediction that the length of the Taylor column slug is $0.675\mathscr{T}$ (see figure 4.2 in Greenspan 1968) may be expected to be relevant to practical cases of

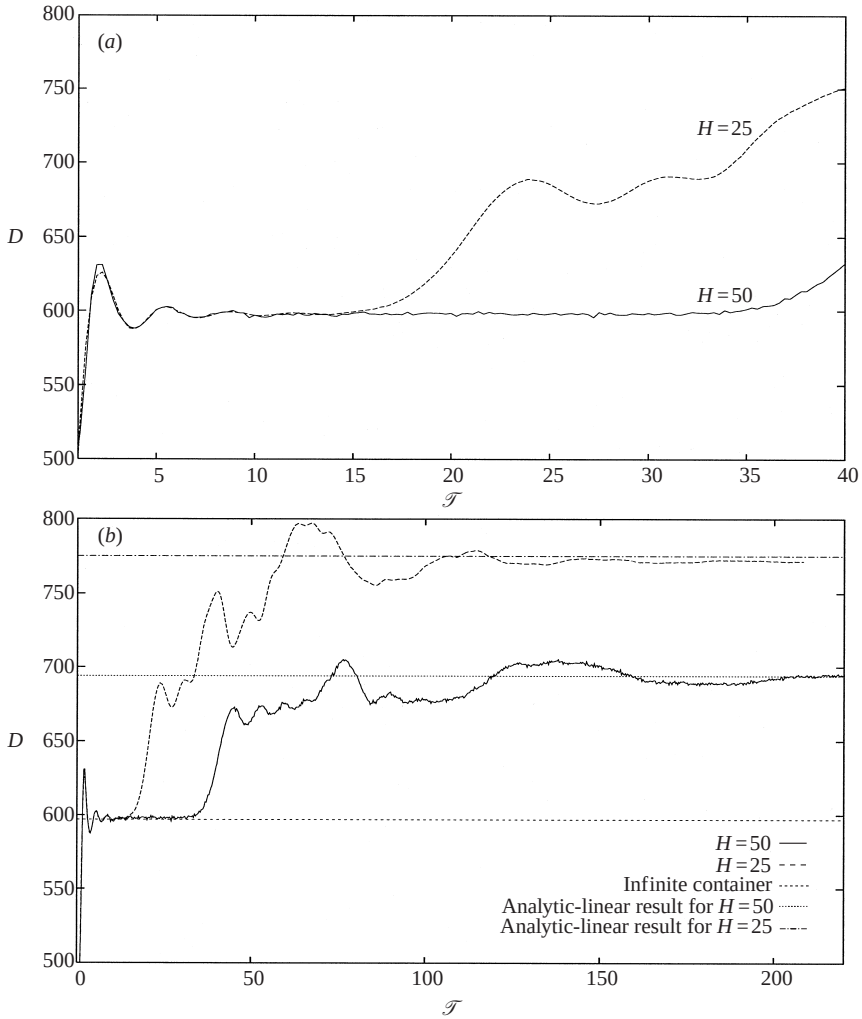

FIGURE 4. The drag force as a function of time, numerical results, for $E = 1/100$, $H = 25$ and $H = 50$, $Ro = 10^{-4}$. Also shown the steady-state analytical-linear results for the infinite and finite containers. (a) A stretched portion of (b).

finite E for a short time period only, $\mathscr{T} < 0.08/E$, until the final length $0.053/E$ is achieved.

Comparisons with numerical results are displayed in figures 5 and 6. The initial growth of the column is in good agreement with Greenspan's inviscid solution. Moreover, the column grows until the steady-state length of the unbounded container is reached, and even slightly overshoots. Next, the length oscillates slightly, with almost inertial frequency, around this value during several revolutions of the system. Then the information about the finiteness of the axial domain reaches the Taylor column and a process of adjustment to the 'correct' steady-state length takes place; during this process quite large-amplitude and low-frequency oscillations appear.

Finally, we found that the time-dependent behaviour of the computed stream functions displays a similar stepwise development, and that the asymmetry of the geometry does not affect the main pattern of the foregoing observations (Minkov 1998).

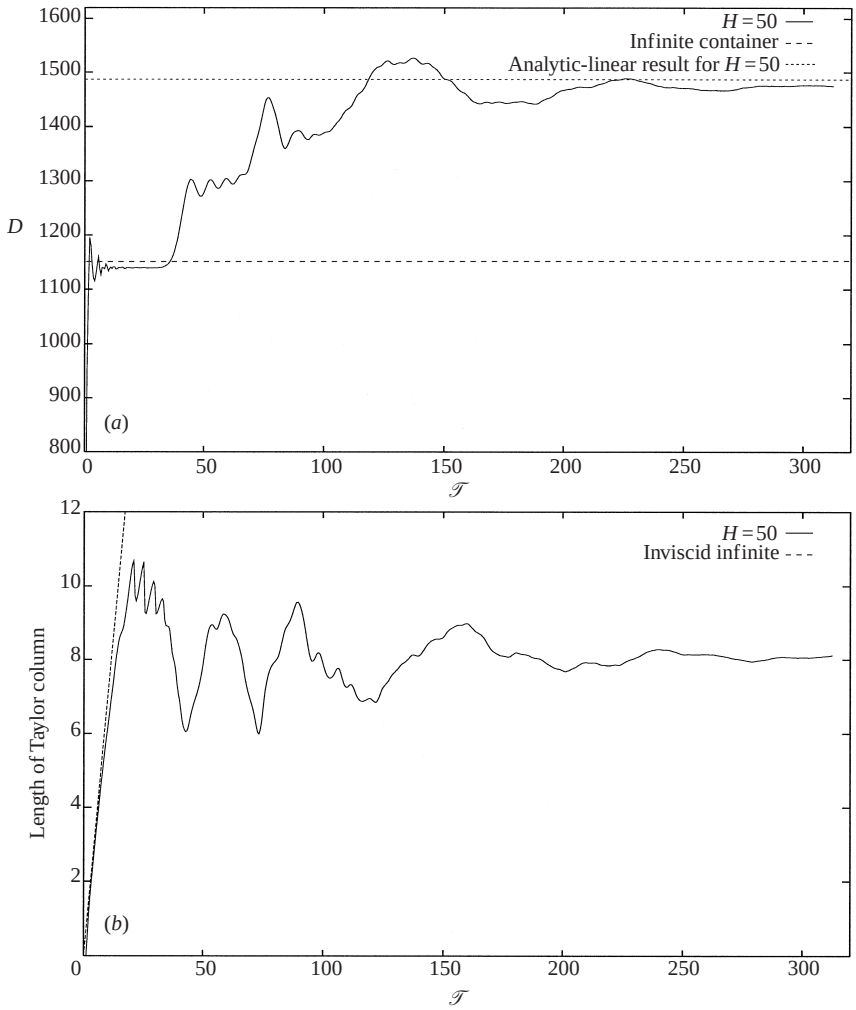

FIGURE 5. The drag force and the length of Taylor column as functions of time, numerical results, for $E = 1/200$, $H = 50$, $Ro = 10^{-4}$. Also shown, in (a), the steady-state analytical-linear drag results for the infinite and finite containers and, in (b), the prediction of Greenspan for the growth of the Taylor column.

The detailed description of the means by which information from the boundaries is conveyed to the Taylor column region, and of the subsequent oscillations, requires a special analysis which is beyond the scope of this paper. However, some standard results of the above-mentioned inertial wave consideration (Greenspan 1968, § 4.3) provide the following tentative interpretation. The fastest wave in our cylindrical container is the one with the longest wavelength, $2r_{max}$, and its group velocity in the axial direction is $2r_{max}/\pi$ (scaled by $\Omega^* a^*$). Such a wave is generated at $t = 0$ at the disk level, then travels from the disk to the horizontal boundary and back (after reflection) in the time interval $\Delta\mathscr{T} = \pi H/r_{max}$. Thus, for the cases with $H = 25$ and 50 considered in the numerical examples, the relevant time intervals are 15.7 and 31.4, respectively. Indeed, figures 4 and 5 indicate that the influence of the horizontal boundaries is first recognized by the drag force at this time, and by the tip of the Taylor column a little earlier. Furthermore, the time interval $\Delta\mathscr{T}$ is in fair agreement

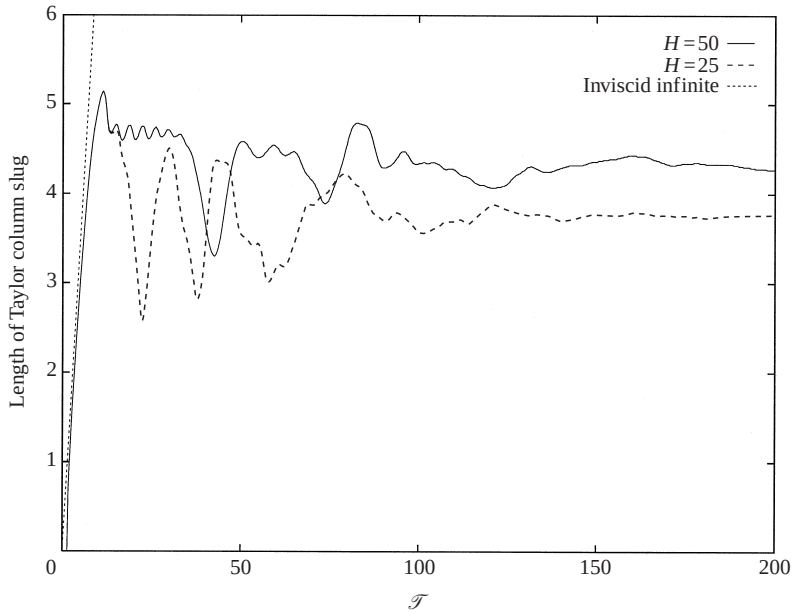

FIGURE 6. The length of Taylor column as a function of time for $E = 1/100$, $H = 25$ and $H = 50$, $Ro = 10^{-4}$ and time-dependent result for the inviscid infinite configuration.

with the period of the large oscillations which accompany the approach to steady state of the Taylor column length. The amplitude of the major oscillations is of the order of magnitude of the difference between the 'finite' and 'infinite' container relevant features. The process is complicated by the viscous decay, wave interactions, and the presence of small-amplitude oscillations with the inertial period π. These inferences are supported well by numerical simulation with various values of r_{max} ranging from 3 to 8 (not displayed here).

We can now estimate the distance z_p travelled by the particle from its initial release until the 'final' steady state is established. We simply multiply the time of the Taylor column formation plus adjustment to the boundary, $0.08/E + 5\Delta\mathscr{T}$, by the constant particle velocity, and obtain

$$\frac{z_p}{H} = Ro\left(\frac{0.08}{EH} + \frac{5\pi}{r_{max}}\right). \tag{2.3}$$

In the typical cases of interest the expression that multiplies Ro is of order unity, and hence for $Ro \ll 1$ a (quasi) steady-state is attainable.

The flow created by starting from rest under the action of a constant force displays a similar behaviour; some details are given in Appendix B.

3. The effect of nonlinear terms

To the best of our knowledge, the effect of the nonlinear terms on the slow motion in a long container has not been investigated theoretically and hence questions about the range of validity of the linear theory, and about the trend of variation of the drag force and the length of the Taylor column when Ro increases from 0 to some small but finite value (say, 0.05), lack theoretical answers.

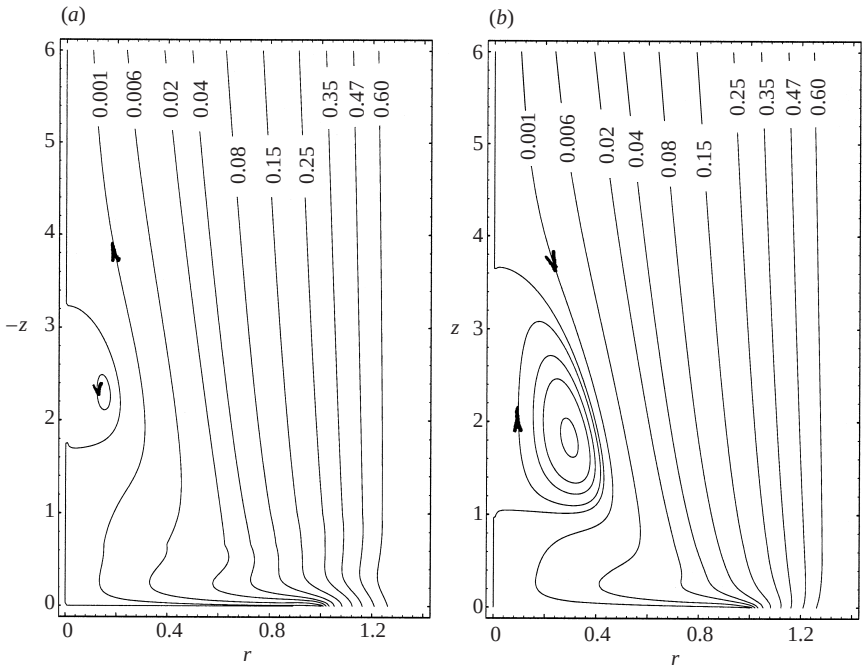

FIGURE 7. The contour lines of the stream function for $E = 1/100$, $H = 25$, $Ro = 0.1$, (a) lower and (b) upper half of flow.

The basic investigation is concerned with the deviations from linear steady-state flow results. Strictly speaking, for $Ro > 0$ the flow field under consideration in a bounded domain has no steady state since the particle–boundary geometry changes with time, and more significantly so when the value of Ro increases. However, we may expect a quasi-steady state when $Ro \ll 1$, as shown in the previous section. On the other hand, in 'numerical experiments' an artificial steady state, with the disk in a fixed position, can be attained for physically unrestricted values of Ro; we think that such virtual boundary conditions results may provide insight into the contribution of the nonlinear terms although they lack a clear-cut physical analogue. This approach was also dictated by a practical numerical difficulty: only computations with $Ro \geqslant 0.02$ show a clear pattern of dependence on the changing Ro which could be viewed as reliable for the present analysis of the nonlinear effects.

Typical results for the lengths of the upper and lower Taylor column slugs and drag force for various values of Ro are presented in tables 3 and 4. Qualitatively, the results indicate that when Ro increases then: (a) the dimensionless drag force decreases and the Taylor column slug shortens; (b) the flow field ahead of and behind the disk becomes asymmetric, with a stronger circulation and longer Taylor column of recirculation on the upper side than on the lower side, see figure 7 (at some larger values of Ro the lower region of trapped recirculating fluid disappears).

Table 3 and figure 8 indicate that the decrease of the dimensionless drag force due to the inertial terms in the long container configurations behaves like Ro^2 for small Ro (say, $Ro \leqslant 0.15$). The accuracy of the coefficient $c = [D - D_{lin}]/[D_{lin}Ro^2]$ is low (two digits for $Ro \geqslant 0.05$ and one digit otherwise) because the values of the drag force for small Ro are close and cancellation errors appear in the numerator. This coefficient increases when H and E decrease. However, we were unable to establish

E	H	Ro	l_u	l_l	$1 - D/D_{lin}$	$(D_{lin} - D)/D_{lin}Ro^2$
1/100	25	0.02	3.7	3.7	0.002	4.9
		0.05	3.7	3.5	0.012	5.0
		0.1	3.6	3.1	0.051	4.9
		0.15	3.4	0	0.11	4.8
		0.2	3.2	0	0.18	4.4
		0.25	3.0	0	0.24	3.8
	50	0.02	4.4	4.4	0.001	3.0
		0.05	4.4	4.3	0.009	3.4
		0.1	4.2	4.0	0.034	3.4
		0.15	3.9	3.5	0.075	3.3
		0.2	3.7	0	0.13	3.2
		0.25	3.3	0	0.18	2.9
1/200	50	0.02	8.1	8.1	0.004	9.4
		0.05	7.9	7.8	0.024	9.5
		0.1	7.4	7.0	0.091	9.1
		0.15	6.8	5.8	0.17	7.6
		0.2	6.2	4.6	0.23	5.7

TABLE 3. Lengths of upper and lower Taylor column slugs and the relative drag force reduction due to the effect of the inertial terms in a finite long container. $l = 0$ means that a stagnation point and region of recirculation did not appear.

E	Ro	l_u	l_l	$1 - D/D_{lin}$	$(D_{lin} - D)/D_{lin}Ro^2$
1/100	0.02	4.7	4.7	0.001	2.1
	0.05	4.6	4.6	0.005	2.4
	0.1	4.5	4.4	0.023	2.4
	0.15	4.2	4.0	0.058	2.6
	0.2	3.9	3.4	0.10	2.5
	0.25	3.6	0	0.15	2.4
	0.33	3.2	0	0.22	2.0
	0.5	2.3	0	0.28	1.1
	0.66	1.6	0	0.26	0.6
1/200	0.02	9.6	9.6	0.002	5.3
	0.05	9.4	9.4	0.012	4.9
	0.1	8.7	8.7	0.050	5.0
	0.15	8.2	7.8	0.11	4.7
	0.2	7.4	6.5	0.16	4.0

TABLE 4. Lengths of upper and lower Taylor column slugs and the relative drag force reduction due to the effect of the inertial terms in a virtual infinite container. $l = 0$ means that a stagnation point and region of recirculation did not appear.

the asymptotical value for $E \to 0, H \to \infty$. We note in this context that the weak dependence of the drag force on Ro is puzzling. An inspection of the numerical results indicates that the advection terms and the resulting changes in the pressure are of the same order of magnitude, but the net contribution to the drag (i.e. the appropriate integral of the pressure difference between the upper and lower sides of the particle) turns out to be nominally much smaller.

The trends of influence of the nonlinear advection terms on the results are consistent with the measurements of Maxworthy (1970), but this conclusion is not straightforward. Figure 11 in that paper shows the length of the Taylor column slug as a

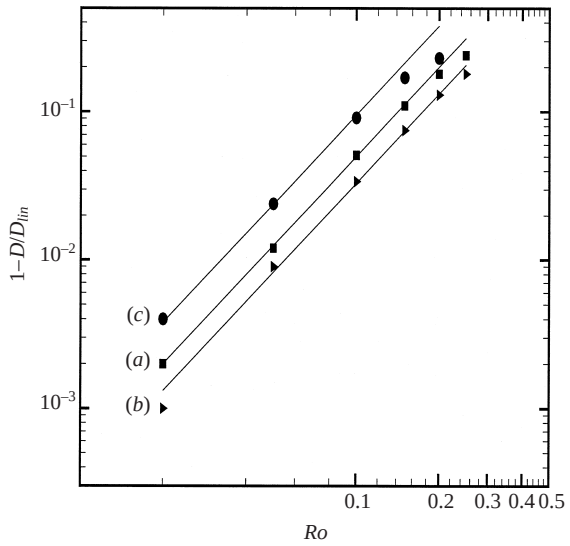

FIGURE 8. The drag force reduction, $1 - D/D_{lin}$, as a function of Ro, numerical results and the cRo^2 fit for (*a*) $E = 1/100$, $H = 25$, $c = 5.0$; (*b*) $E = 1/100$, $H = 50$, $c = 3.3$; (*c*) $E = 1/200$, $H = 50$, $c = 9.5$.

function of the parameter $2/Ro$ for various values of $1/66 \leqslant E \leqslant 1/375$. (In the original notation the parameter N equals $2/Ro$ in our notation.) The impression is that for a fixed value of E the length of the column decreases with Ro, although the rate of change becomes less pronounced as E decreases. However, on p. 469 Maxworthy states that the length of the column does not change with Ro (in the range 0.02–0.4) for 'small enough' values of E. Our results indicate a decrease of the length with Ro for the tested values of $E = 1/100$ and $1/200$. Maxworthy presented the drag results the form $C_D = (2/\pi)DE/Ro$ in our notation. For small E the experiment gave $C_D \sim 1/Ro^{1.07}$, i.e. D decreases as $1/Ro^{0.07}$ when Ro increases for a fixed E. A good comparison with the numerical trend $D \sim (1 - cRo^2)$ would need accurate values of $C_D \times Ro$ which cannot be extracted from the log-log plots of C_D vs. $2/Ro$ of the paper.

In any case, the major discrepancy between theory and these experiments concerning the value of the drag force remains unresolved, and becomes even more puzzling in view of the present results. The measured drag values (for a sphere) are significantly larger than the analytical-linear ($Ro = 0$) predictions, which seemed to suggest that either the analytical-linear $Ro = 0$ results are wrong, or the dimensionless drag increases significantly due to the presence of advection terms in the real flows. But our numerical results clearly refute these possibilities, by showing that the linear results are correct (for small values of Ro) and the incorporation of the nonlinear terms reduces the dimensionless drag.

4. Concluding remarks

We performed a numerical investigation, based on the the full axisymmetric Navier–Stokes equations, of the flow field generated by a disk particle that moves slowly along the axis in a long rapidly rotating cylindrical container.

We investigated both (quasi) steady state and the initial transient stage.

Comparisons of numerical solutions with $Ro = 10^{-4}$ to linear ($Ro = 0$) quasi-

steady analytical solutions were performed. For the symmetric geometry (particle in the midplane) good agreement was obtained with the results of UV and VU. This is a strong support of the view that the linear theory is a regular limit of the $Ro \ll 1$ solution, and hence the insight provided by the linear theory into the Taylor column slug structure and drag force behaviour have physical relevance (although strictly speaking, $Ro = 0$ means no motion). For a non-symmetric configuration we introduced and tested a simple conjecture for the analytical calculation of the drag force by combining available linear results for simpler cases: the $E \to 0$ case studied by Hocking *et al.* (1979) and the unbounded-domain 'exact' results of VU. We suggest that this conjecture can also be applied to spherical and ellipsoidal particle by using the unbounded-domain 'exact' results of Tanzosh & Stone (1994). This provides an extension of the predictive power of the linear theory: the drag for a finite (but small) value E when the particle is in a non-symmetric position in a long container can be accurately evaluated (although no direct analytical solution to this geometry is available).

We investigated the time-dependent initial stage of formation of the flow field for both an impulsive start and release from rest under the action of a constant axial force. In both cases a novel behaviour has been detected: first the flow field attains and maintains for a while the steady-state values of the unbounded configuration. The time period of this first stage is $\Delta\mathscr{T} \approx \pi H/r_{max}$ (in the asymmetric situation, the smallest of H_u, H_l replaces H), which, in some feasible circumstances, corresponds to several revolutions of the system. This gives physical reality to the abstract 'unbounded domain' solution. During this stage, a particle released under a constant force is expected to overshoot the steady-state velocity. In the second stage the flow field around the disk 'feels' the influence of the horizontal boundaries and readjusts, with oscillations, to the steady state in the bounded configuration (i.e. a shorter Taylor column slug and a larger drag force). These stages are consistent with the axial propagation of perturbations by inertial waves of two typical lengths: of the disk diameter, to form the Taylor column, and of the container diameter, to adjust to the presence of the horizontal walls; although the latter waves travel faster, their influence is delayed when the container is much longer than the Taylor column.

The effect of the nonlinear advection terms in a long container configuration was an open question, to which our computations, for small but finite value of Ro, provide the following answers. When Ro increases from 'zero' to larger values, the dimensionless drag force decreases (some care is needed in the interpretation because the drag is scaled with $\rho^* v^* a^* W^*$). The difference between the linear and the nonlinear dimensionless drag results is proportional to Ro^2. Additional investigation is needed for explaining and perhaps better quantifying this feature. In this regime, the upper Taylor column of trapped fluid is slightly shorter and wider than the linear predictions, and the lower Taylor column slug is significantly shorter and thiner than the linear one. When Ro is increased above some 'critical' value the influence of this parameter on the drag force becomes milder, and the lower region of recirculation may disappear. The theoretical restriction on the linear theory is $Ro \ll 1$ (in contrast with the more restrictive $RoE^{-1/2} \ll 1$ in the short container).

Contrary to expectations, the present solution does not bridge the gap between the theoretical linear drag prediction and the larger experimental result of Maxworthy (1970), because the nonlinear terms reduce the force and actually increase the discrepancy. Since non-axisymmetric components and instabilities were not incorporated in our investigation, these effects are obvious candidates for a possible increase of the theoretical drag.

A deficiency of the present investigation is the shape of the particle, which is a thin disk. No experimental data are available for such a geometry (which adds control difficulties to the many practical problems encountered in the experiments with spherical particles). However, there are strong theoretical indications that for the considered configuration the essential flow-field features for disk, spherical and ellipsoidal (with non-large length/radius value) particles are very similar, because the Taylor column is much longer than the particle dimensions and the drag is mostly contributed by the pressure difference. Nevertheless, the numerical solution for a spherical and ellipsoidal particle is of interest to complete the knowledge on the problem. Other significant generalizations of the present problem that could benefit from a numerical investigation concern (*a*) the motion of a drop and (*b*) the motion of two or more particles (see Davis & Stone 1998). These problems, however, require major modifications of the present code.

The present progress in theory suggests the need of new experiments. Experimental clear-cut verification of the shape of the Taylor column slug and the recirculation inside it, the influence of *Ro*, the asymmetry and the time-dependent stage are expected to strengthen our knowledge and resolve the drag value discrepancy. Experimental observations on interactions between two (and more) particles are expected to point out novel and perhaps fascinating effects.

The research was partially supported by the Fund for the Promotion of Research at the Technion and by the Bar-Nir Bergreen Software Technology Center of Excellence. The comments of prof. H. P. Greenspan are appreciated.

Appendix A. The boundary influence function of Hocking *et al.*

Values of the function $G(\delta_t, \delta_b)$ are given below. Recall that

$$\delta = HE = \tfrac{1}{2}(\delta_b + \delta_t) \tag{A 1}$$

and $G(\delta_t, \delta_b) = G(\delta_b, \delta_t)$.

The diagonal values are for the symmetric $\delta_b = \delta_t = \delta$ in which case $G(\delta, \delta) = F(\delta)$.

δ_b, δ_t	0.25	0.30	0.35	0.40	0.45	0.50	0.55	0.60	0.65	0.70	0.75	0.80	0.85	0.90	0.95
0.25	1.318														
0.30	1.295	1.269													
0.35	1.279	1.252	1.233												
0.40	1.267	1.239	1.220	1.206											
0.45	1.259	1.230	1.210	1.196	1.185										
0.50	1.253	1.224	1.203	1.188	1.176	1.167									
0.55	1.249	1.218	1.197	1.181	1.170	1.160	1.153								
0.60	1.245	1.214	1.192	1.176	1.164	1.155	1.147	1.141							
0.65	1.242	1.211	1.189	1.172	1.160	1.150	1.142	1.136	1.131						
0.70	1.240	1.208	1.186	1.169	1.156	1.146	1.138	1.132	1.127	1.122					
0.75	1.238	1.206	1.183	1.166	1.154	1.143	1.135	1.128	1.123	1.118	1.114				
0.80	1.237	1.204	1.181	1.164	1.151	1.141	1.132	1.126	1.120	1.115	1.111	1.108			
0.85	1.235	1.203	1.180	1.162	1.149	1.138	1.130	1.123	1.117	1.112	1.108	1.105	1.102		
0.90	1.234	1.202	1.178	1.161	1.147	1.137	1.128	1.121	1.115	1.110	1.106	1.102	1.099	1.096	
0.95	1.233	1.201	1.177	1.159	1.146	1.135	1.126	1.119	1.113	1.108	1.104	1.100	1.097	1.094	1.092

Appendix B. Constant driving force

The time-dependent flow field which appears when the particle is set in motion from rest under the action of a constant force (in contrast with the impulsive start) is of interest. This is expected to provide a good approximation to the physical situation of a buoyant particle which is released from rest at some position along an axis of rotation parallel to the gravitational acceleration. The experiments of Maxworthy (1970) were performed in this way with spherical particles lighter than the surrounding water. Unfortunately, no record of the initial stage of motion was made, the main concern of these experiments being the (supposedly attainable) quasi-steady state. Furthermore, to our best knowledge, no theoretical study of this problem has been performed.

For the numerical solution of this problem the previously used finite-difference code was modified, since the value of the time-dependent velocity of the particle relative to the horizontal boundaries, w_p, is sought as a part of the problem.

For the calculation of this additional variable we add the equation of motion of the particle to the Navier–Stokes equations and previously defined boundary conditions. The total force acting on the particle is the constant external (say, the effective buoyancy) force minus the instantaneous drag force, $D^*(t^*)$, which depends on the instantaneous flow field around the particle. As in the previous case, we scale the velocities with the particle velocity at the steady state, so the steady state has to be identical to the case of an impulsive start. This means that the external force is equal to the drag force at the steady state, $D^*(\infty)$, which can be computed from the impulsive start configuration. The mass m_p^* of the particle is considered here as a known, controllable, positive constant quantity. This adds one free parameter to Ro, E and H that govern the flow in the quasi-steady state.

The additional equation is in dimensionless form

$$m_p \frac{\mathrm{d}w_p}{\mathrm{d}\mathscr{T}} = D(\infty) - D(\mathscr{T}). \tag{B 1}$$

Here, again, $\mathscr{T} = t^*\Omega^*$ and the dimensionless mass is scaled as

$$m_p = m_p^* \frac{\Omega^*}{\nu^* \rho^* a^*}. \tag{B 2}$$

In this scaling, if the dimensional mass of the particle is $m_p^* = A\rho^* a^{*3}$, where A is a non-dimensional positive constant of the order of unity, its dimensionless mass will be $m_p = AE^{-1}$. For example, the dimensionless mass of a spherical particle with the same density as the fluid, ρ^*, is $m_p = \frac{4}{3}\pi E^{-1}$. In the present long container configuration the right-hand side of (B 1) is $O(E^{-1})$ and hence an $O(1)$ acceleration of the particle is expected on the $\mathscr{T}$ time scale.

The time-dependent solution of the flow field is now coupled with the solution of (B 1). The necessary modification of the numerical scheme is described in Part 1.

A typical result is shown in figure 9 for a container of $H = 50$ and two values of E. The axial velocity w_p of the particle increases smoothly from 0 to 1 in less than one revolution of the container, but overshoots this value, reaches and maintains for a while a distinctive maximal value till about $\mathscr{T} = 35$, then decreases towards the steady-state value 1. This behaviour is consistent with that for the impulsive start. Initially, the drag force on the particle grows (in about one revolution) to the value predicted for the unbounded container, which is smaller than that of the steady state in the finite container (by 13% for the larger E and 17% for the smaller E). Since

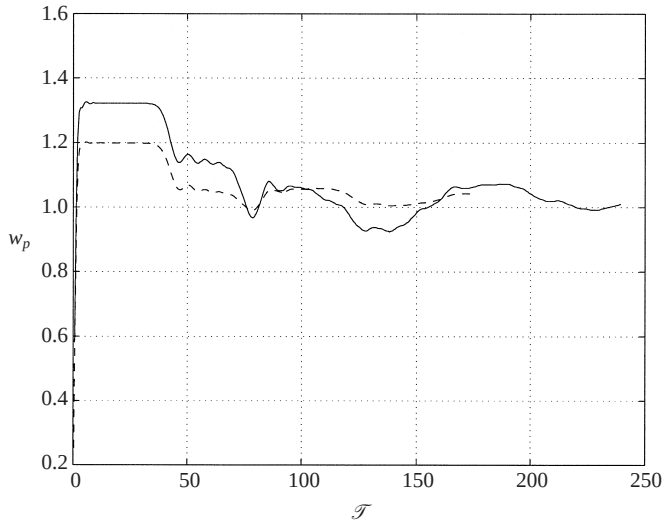

FIGURE 9. The particle velocity as a function of time for motion under constant driving force with $H = 50$, $Ro = 10^{-4}$ for $E = 1/100, m_p = 419$ (dashed line) and $E = 1/200, m_p = 838$ (solid line).

the magnitude of the buoyant force is set equal to the steady-state drag, the particle maintains a positive acceleration even after reaching $w_p = 1$. At about $\mathscr{T} = 35$ the information from the boundaries reaches the particle. This time interval is in agreement with $\Delta\mathscr{T} = \pi H/r_{max} = 31.4$ estimated from the propagation of the inertial wave in the impulsive start. After the start of the influence from the horizontal boundaries the drag increases to the larger value which corresponds to the bounded container and is in exact balance with the constant buoyancy force. The velocity is therefore reduced to the steady-state value of 1.

REFERENCES

BARNARD, B. J. S. & PRITCHARD, W. G. 1975 The motion generated by a body moving through a stratified fluid at large Richardson numbers. *J. Fluid Mech.* **71**, 43–64.

DAVIS, A. M. J. & STONE, H. A. 1998 Slow translation, rotation or oscillation of a disk in a rotating fluid: effect of a plane wall or another disk. *Q. J. Mech. Appl. Maths* **51**, 495–513.

DENNIS, S. C. R., INGHAM, D. B. & SINGH, S. N. 1982 The slow translation of a sphere in a rotating viscous fluid. *J. Fluid Mech.* **117**, 251–267.

GREENSPAN, H. P. 1968 *The Theory of Rotating Fluids*. Cambridge University Press.

HOCKING, L. M., MOORE, D. W. & WALTON, I. C. 1979 The drag on a sphere moving axially in a long rotating container. *J. Fluid Mech.* **90**, 781–793.

MAXWORTHY, T. 1970 The flow created by a sphere moving along the axis of a rotating, slightly-viscous fluid. *J. Fluid Mech.* **40**, 453–479.

MINKOV, E. 1998 A numerical study of the flow around particles in rotating fluid. PhD Thesis, Technion.

MINKOV, E., UNGARISH, M. & ISRAELI, M. 2000 The motion generated by a rising particle in a rotating fluid – numerical solutions. Part 1. The short container case. *J. Fluid Mech.* **413**, 111–148.

MOORE, D. W. & SAFFMAN, P. G. 1969 The structure of free vertical shear layers in a rotating fluid and the motion produced by a slowly rising body. *Phil. Trans. R. Soc. Lond.* A **264**, 597–634.

MORRISON, J. W. & MORGAN, G. W. 1956 The slow motion of a disk along the axis of viscous, rotating liquid. *Rep.* 56207/8. Div. of Appl. Maths, Brown University.

Smith, S. H. 1987 The formation of Stewartson layers in a rotating fluid. *Q. J. Mech. Appl. Maths* **40**, 575–594.

Stewartson, K. 1952 On the slow motion of an ellipsoid in a rotating fluid. *Q. J. Mech. Appl. Maths* **6**, 141–162.

Tanzosh, J. & Stone, H. A. 1994 Motion of a rigid particle in a rotating viscous flow: An integral equation approach. *J. Fluid Mech.* **275**, 225–256.

Taylor, G. I. 1922 The motion of sphere in a rotating liquid. *Proc. R. Soc. Lond.* A **102**, 180–189.

Taylor, G. I. 1923 Experiments on the motion of solid bodies in rotating fluids. *Proc. R. Soc. Lond.* A **104**, 213–218.

Ungarish, M. 1993 *Hydrodynamics of Suspensions.* Springer.

Ungarish, M. & Vedensky, D. 1995 The motion of a rising disk in a rotating axially bounded fluid for large Taylor number. *J. Fluid Mech.* **291**, 1–32 (referred to herein as UV).

Vedensky, D. & Ungarish, M. 1994 The motion generated by a slowly rising disk in an unbounded rotating fluid for arbitrary Taylor number. *J. Fluid Mech.* **262**, 1–26 (referred to herein as VU).

Weisenborn, A. J. 1985 Drag on a sphere moving slowly in a rotating viscous fluid. *J. Fluid Mech.* **153**, 215–227.